

PACS numbers: 33.50.–j; 42.30.Wb; 87.57.–s
DOI: 10.1070/QE2010v040n06ABEH014278

Spectrally resolved fluorescence diffuse tomography of biological tissues

M.S. Kleshnin, I.V. Turchin

Abstract. **Spectrally resolved fluorescence diffuse tomography (SFDT) is demonstrated to be an effective approach to the reconstruction of the fluorescent agent distribution in biological tissues. Analysis of the measured optical power spectrum enables more accurate fluorophore localisation in solving the inverse tomography problem, because the dispersion of the optical parameters of the imaging subject leads to characteristic changes in the shape of its fluorescence spectrum. The SFDT system built by us includes a common optical fibre output of light sources and a single fibre input of the detector in an on-axis configuration, and an electromechanical scanner. The system enables studies of laboratory animals having tumours labelled with various fluorescent agents (fluorescent proteins, quantum dots and others). The first *in vivo* experiments have demonstrated the feasibility of tumour detection and localisation in laboratory animals by SFDT.**

Keywords: *fluorescence diffuse tomography, fluorescent proteins, dispersion of the optical parameters of biological tissues, fluorophore distribution reconstruction.*

1. Introduction

One promising area of research in modern experimental oncology is the development of optical techniques for noninvasive imaging of the growth, regression and metastasis of malignancies in response to antitumour therapy. Recent years have seen widespread interest in fluorescence techniques for visualising the internal structure of biological tissue, due to the advent of high-power compact laser sources operating at various wavelengths, high-sensitivity optical detectors and novel bright contrast agents such as fluorescent proteins. Fluorescent-protein genes can be transfected into human tumour cells, which are then implanted into an experimental animal. The ability to fluoresce in a transfected cell persists throughout its life and after cell division, which offers new opportunities in solving a variety of problems: from investigation of structural and functional disorders underlying various diseases to the development of new effective drug testing methods.

Fluorescence techniques for visualising the inner structure of biological tissue include surface imaging, projection tomographic imaging and fluorescence diffuse tomography (FDT). Surface imaging [1] makes it possible to rapidly (1 – 5 s) estimate the cross-sectional size of surface tumours by exposing the imaging subject to a broad homogenised light beam. The accuracy of such estimates is higher when the tumour is closer to the surface: the image of a deep-seated tumour is considerably blurred because of the strong light scattering in biological tissues. Projection imaging [2] offers the possibility of recovering a two-dimensional (2D) image (projection) of tissue at a given arrangement of narrow-beam sources and detectors using transillumination. As distinct from that of surface imaging, the resolving power of projection imaging is less dependent on tumour depth, but this approach is more difficult to implement, and the data acquisition time may reach several minutes. FDT [3] enables 3D imaging of fluorescing tumours using a set of different projections of the tissue. FDT provides the most accurate information about the tumour size and location in a laboratory animal, but the reconstruction of the fluorescent agent distribution in biological tissue requires an algorithm that takes into account the specifics of the system, the design and operating principle of the experimental setup, the type of the fluorophore, etc.

The internal structure of tissue can be reconstructed using data collected in a series of measurements at different positions of the light source and detector relative to the imaging subject [4, 5]. As a rule, use is made of intensity data obtained at each position of the detector. In the optical range, biological tissues are strong scatterers [6], which leads to significant broadening of the beam (in contrast to X-ray tomography, where photons have straight paths). This adds a great deal of complexity to the fluorophore distribution reconstruction, so the search for and development of various approaches to gaining additional information about the location of fluorescent regions is an important issue. There are time-domain [7, 8] (output pulse duration and shape measurements) and frequency-domain [9] (determination of the phase of intensity-modulated radiation) FDT approaches, capable of providing additional information. However, the implementation of the time-domain approach requires sophisticated, expensive light sources and detectors, such as picosecond lasers and high-speed CCD cameras. The depth of fluorescent inclusions can also be inferred from the spectrum of the fluorescence signal using spectrally resolved FDT (SFDT) [10].

M.S. Kleshnin, I.V. Turchin Institute of Applied Physics, Russian Academy of Sciences, ul. Ulyanova 46, 603950 Nizhnii Novgorod, Russia; e-mail: m_s_kleshnin@list.ru

Received 21 January 2010
Kvantovaya Elektronika **40** (6) 531 – 537 (2010)
Translated by O.M. Tsarev

The main parameters describing the propagation of optical radiation in biological tissue are the transport scattering coefficient, μ_s', and absorption coefficient, μ_a. In contrast to the transport scattering coefficient, the absorption coefficient has strong dispersion in the range 500 – 700 nm, which leads to changes in the spectrum of the light propagating through the tissue. The associated distortion of the spectral shape can be used to assess the depth of the fluorescent region in the imaging subject (SFDT method).

The higher the dispersion and the longer the path in the dispersing medium, the stronger is the distortion of the measured spectrum and, hence, the higher can be the accuracy in fluorophore distribution reconstruction. However, in the range of their highest optical dispersion (500 – 600 nm), biological tissues exhibit strong light absorption, which considerably hinders detection of the transmitted light. Because of this, the optimal spectral range for SFDT imaging of biological objects 1 – 2 cm in thickness (small laboratory animals) is 600 – 700 nm, where the dispersion of the absorption coefficient is sufficiently high, whereas the attenuation of light in such media is not very strong. In addition, recent years have seen the advent of red fluorescent proteins that offer high fluorescence brightness in this spectral range (Fig. 1) [11].

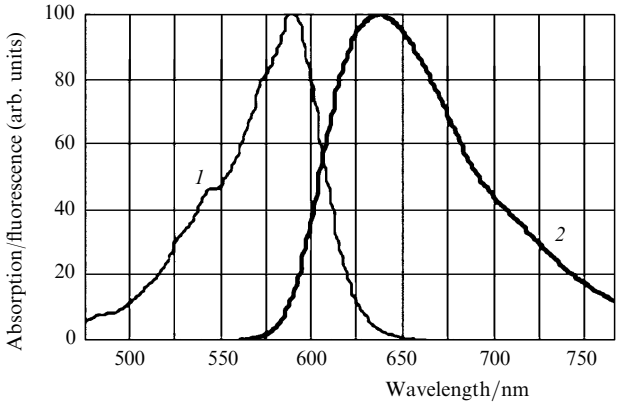

Figure 1. Normalised (*1*) absorption and (*2*) fluorescence spectra of the TurboFP635 protein.

The SFDT approach was first implemented for a homogeneous, strongly scattering medium with known optical parameters, containing fluorescent inclusions [12]. Numerical simulation and experimental studies with biological phantoms have demonstrated the feasibility of using SFDT in the spectral range of high optical dispersion, but no *in vivo* studies of biological objects have been performed to date.

We have designed an experimental setup for SFDT imaging of fluorescently labelled tumours in laboratory animals. In includes a common fibre output of light sources and a single fibre input of the detector in an on-axis configuration, and an electromechanical scanning system. As a probe radiation source, we use a laser which excites a fluorescent agent. The transmitted optical power spectrum is monitored with a high-sensitivity cooled spectrometer. The absorption spectrum of biological tissue is obtained by scanning the white light source over the surface of the imaging subject. This SFDT system was used to perform the first *in vivo* experiments aimed at localising a fluorescing tumour in a laboratory animal. The results demonstrate that the proposed SFDT method is a viable approach to *in vivo* tumour detection and localisation in laboratory animals.

2. Model of light propagation in biological tissues

To describe light propagation in biological objects whose size exceeds the photon mean free path by several orders of magnitude, we use the diffusion approximation of the radiative transfer equation for a homogeneous, strongly scattering medium. In this approximation, the spectral intensity of light propagating in a medium from a point source is given by [12, 13]

$$E(\boldsymbol{r}_0,\boldsymbol{r},\lambda)=\frac{3P_0[\mu_s'(\lambda)+0.55\mu_a(\lambda)]}{4\pi|\boldsymbol{r}_0-\boldsymbol{r}|}\times\exp[-\{3\mu_a(\lambda)[\mu_s'(\lambda)+0.55\mu_a(\lambda)]\}^{1/2}|\boldsymbol{r}_0-\boldsymbol{r}|],\quad(1)$$

where P_0 is the incident spectral power; $\boldsymbol{r}_0$ is the radius vector of the light source; $\boldsymbol{r}$ is the radius vector of an arbitrary point in the medium; and λ is the radiation wavelength. The spectral power of the detected fluorescence is then

$$P(\boldsymbol{r}_s,\boldsymbol{r}_d,\lambda)=\int_V K(\boldsymbol{r})F(\lambda)E(\boldsymbol{r}_s,\boldsymbol{r},\lambda_{las})\frac{\gamma}{P_0}E(\boldsymbol{r},\boldsymbol{r}_d,\lambda)\mathrm{d}\boldsymbol{r}.\quad(2)$$

Here, γ takes into account the active area of the detector and the quantum yield and absorption cross section of the fluorophore; $\boldsymbol{r}_s$ is the radius vector of the excitation source; $\boldsymbol{r}_d$ is the radius vector of the detector; λ_{las} is the excitation wavelength; $K(\boldsymbol{r})$ is the fluorophore concentration distribution; $F(\lambda)$ is the normalised spectral fluorescence intensity; and V is the volume of the imaging subject. It is seen from the relations above that, knowing the detected power, one can numerically solve the integral equation (2) for the unknown kernel. The inhomogeneity of biological tissues hinders fluorophore distribution reconstruction, but the problem can be simplified in a number of cases.

In the case of a plane-parallel object homogeneous in the sensitivity region of the detector and an on-axis arrangement of the source and detector (Fig. 2), relation (1) for the spectral intensity takes the form

$$E(x,y,z,\lambda)_{(x,y)\in\Omega}=\frac{3P_0[\mu_s'(\lambda)+0.55\mu_a(\lambda)]}{4\pi z}\times\exp[-\{3\mu_a(\lambda)[\mu_s'(\lambda)+0.55\mu_a(\lambda)]\}^{1/2}z],\quad(3)$$

were x, y, and z are the coordinates of a point in the sensitivity region of the detector and Ω is the cross-sectional area of the sensitivity region in a plane parallel to the boundaries of the object.

Excitation of the object may cause not only target fluorescence but also fluorescence in the surrounding biological tissues (autofluorescence in fluorescence imaging of biological objects), which will contribute to the distortion of the detected optical power spectrum. Therefore, in the model above, the spectral fluorescence power corrected for autofluorescence is given by

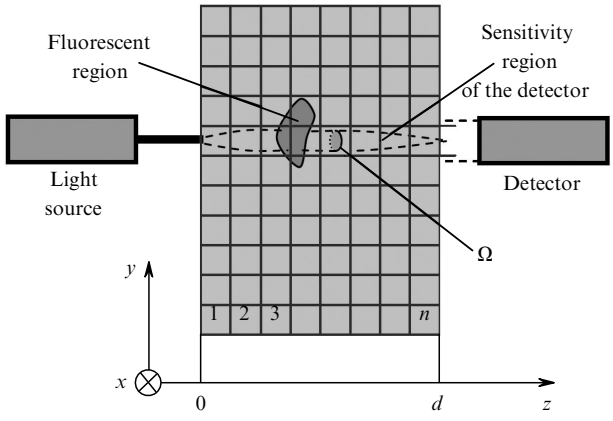

Figure 2. Geometry of light propagation in biological tissue.

$$P(x,y,\lambda) = \int_0^d [K(x,y,z)F(\lambda) + N(x,y,z)A(\lambda)]$$

$$\times E(x,y,z,\lambda_{las})\frac{\gamma}{P_0}E(x,y,d-z,\lambda)\mathrm{d}z. \quad (4)$$

Here, $N(x,y,z)$ is the number density of autofluorescent inclusions; $A(\lambda)$ is the normalised spectral autofluorescence intensity; and d is the thickness of the object.

Note that the planar model we use substantially simplifies the boundary conditions for the integral equation (4), which can be derived using virtual mirror image sources [14].

3. Experimental setup for SFDT

The SFDT system is shown schematically in Fig. 3a. It includes a laser source, white light source, photodetector and electromechanical scanner. The common fibre output of the light sources and the single fibre input of the detector are arranged in an on-axis configuration. The radiation from the laser source (SDL-593-200T, Shanghai Dream Lasers Technology Co., Ltd., P.R. China) passes through the output fibre coupler and impinges on the imaging subject, causing fluorescence of fluorophore-labelled regions. The fluorescence is collected by the fibre input of the detector (QE65000 spectrometer, Ocean Optics Inc., USA). The electromechanical scanning system enables synchronous translation of the fibre output of the light sources and the fibre input of the detector in the plane of the imaging subject with an arbitrary step between neighbouring fluorescence measurement points. The absorption spectrum of the biological tissue is obtained by scanning the white light source (PX-2 xenon lamp, Ocean Optics Inc., USA) over the surface of the imaging subject. The experimental animal is fixed between two glass plates. The fixing post is situated between the source and detector.

To gain additional information that would allow the autofluorescence of the biological tissue to be taken into account, the object is scanned in two different positions (Figs. 3b, 3c), one arbitrary and the other obtained by rotating the object around the vertical axis through 180°. The fluorescent region is closer to the source in one of the scans and to the detector in the other.

The SFDT system was used to perform the first *in vivo* experiments aimed at localising a fluorescing tumour in a laboratory animal (nude mouse, Fig. 3f). The marker used was the TurboFP635 fluorescent protein (Fig. 1) [15]. Scanning results are represented as a 2D image at a particular wavelength. The image corresponds to the main projection (the source and detector on the same axis) of the imaging subject (Figs. 3d, 3e). Other projections can be obtained by scanning the object at different displacements of the source from the detector axis.

4. Fluorophore distribution reconstruction by SFDT

To obtain the absorption spectrum at each point of the scan area, we use relation (3) for spectral intensity in the form

$$\frac{4\pi E(x,y,d,\lambda)_{(x,y)\in\Omega}}{3P(\lambda)} = \frac{\mu_s'(\lambda)+0.55\mu_a(\lambda)}{d}$$

$$\times \exp[-\{3\mu_a(\lambda)[\mu_s'(\lambda)+0.55\mu_a(\lambda)]\}^{1/2}d], \quad (5)$$

where $P(\lambda)$ is the spectral power of the incident white light. Relation (5) for a given λ value can be interpreted as an algebraic equation in two unknowns (μ_s' and μ_a), which has an infinite set of solutions. Since Eqn (5) is valid for any thickness of the imaging subject, a partial solution for a given thickness is sufficient to reconstruct the fluorophore distribution. Therefore, the wavelength dependence of the transport scattering coefficient can be represented analytically, and the absorption spectrum can be determined from relation (5) using experimental data (Fig. 4).

To reconstruct the fluorophore distribution in the imaging subject by SFDT, one must solve the integral equation (4). To this end, the volume of the object is divided into elements (Fig. 2) and integration is replaced by summation. If the cross-sectional size of the sensitivity region, Ω, does not exceed that of the volume elements, the integral equation (4) reduces to the system of linear equations

$$P_{ij}^{s}(\lambda_m) = \sum_{k=1}^{n} f_{ij}(z_k,\lambda_m)$$

$$\times[K(x_i,y_j,z_k)F(\lambda_m) + N(x_i,y_j,z_k)A(\lambda_m)],$$

$$P_{ij}^{d}(\lambda_m) = \sum_{k=1}^{n} f_{ij}(d-z_k,\lambda_m)\times$$

$$\times[K(x_i,y_j,z_k)F(\lambda_m) + N(x_i,y_j,z_k)A(\lambda_m)],$$

$$z_k = \frac{2k-1}{2n}d, \quad m = 1,2,3,...,M, \quad (6)$$

where n is the total number of volume elements; M is the number of wavelengths used; $P_{ij}^{s}(\lambda_m)$ and $P_{ij}^{d}(\lambda_m)$ are the spectral emission powers detected at point (x_i, y_j) and wavelength λ_m for two positions of the object [the tumour closer to the source (Fig. 3b) or to the detector (Fig. 3c)]; and $f_{ij}(z_k,\ \lambda_m)$ are the coefficients of the system of equations:

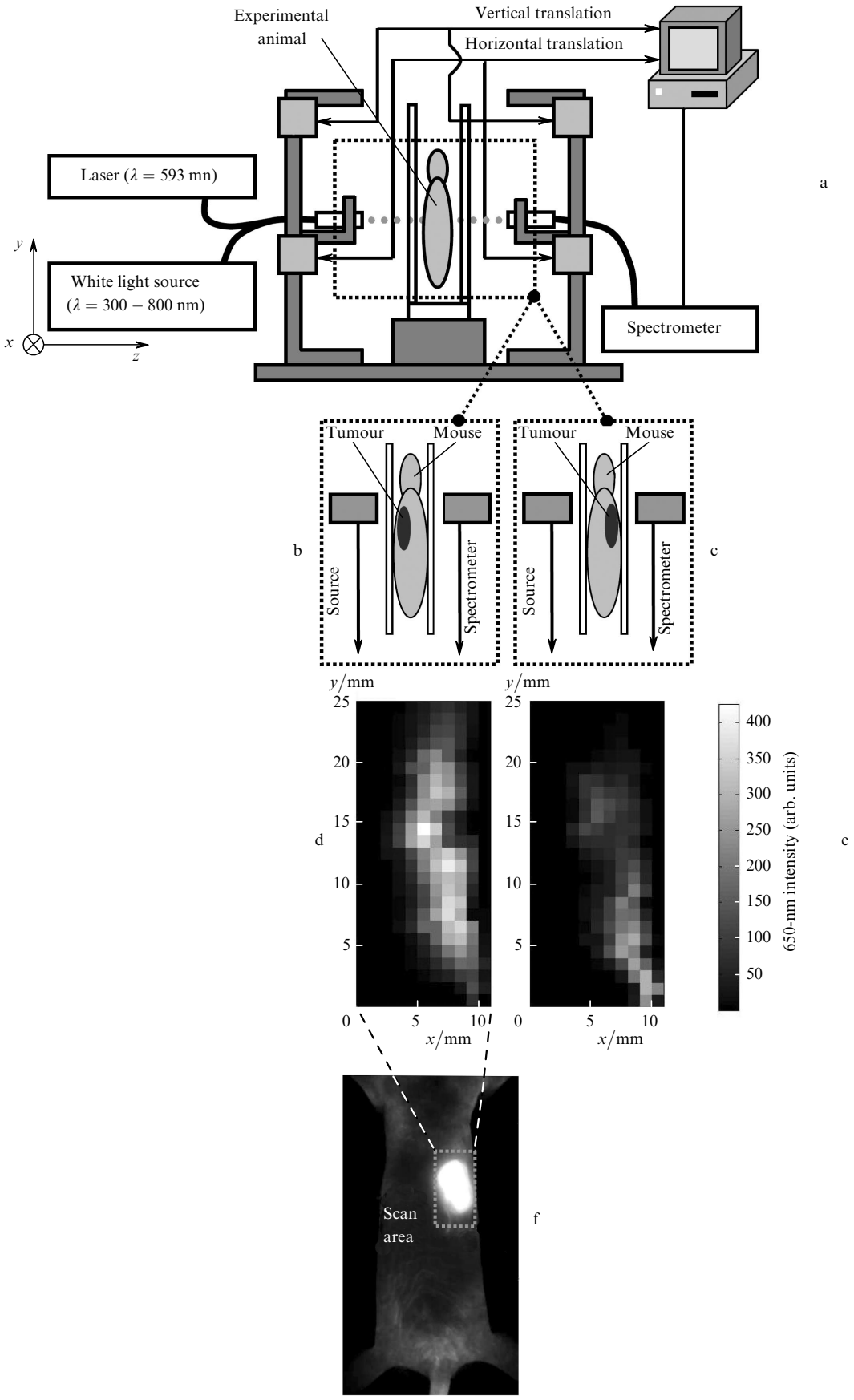

Figure 3. (a) Schematic of the experimental setup; (b, c) imaging subject with the tumour located closer to the light source and detector, respectively; (d, e) spectral fluorescence intensity maps of the scan area for the above tumour positions, respectively; (f) imaging subject and scan area.

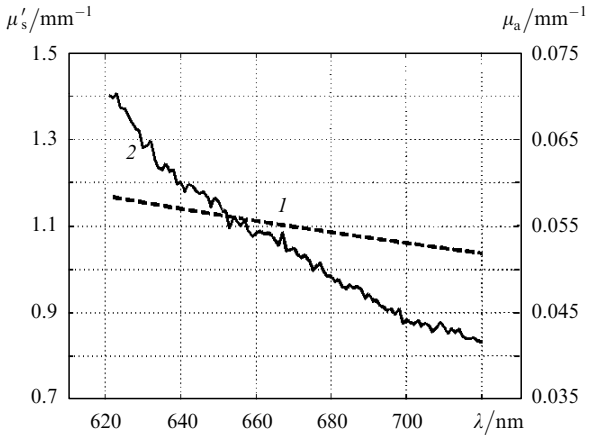

Figure 4. (*1*) Analytical fit for the transport scattering coefficient $\mu'_s(\lambda)$ [12] and (*2*) spectral dependence of the absorption coefficient, $\mu_a(\lambda)$, at one point in the scan area ($x = 6$ mm, $y = 6$ mm).

$$f_{ij}(z_k, \lambda_m) = \frac{\gamma}{P_0} E(x_i, y_j, z_k, \lambda_{las}) E(x_i, y_j, d - z_k, \lambda_m). \qquad (7)$$

These matrix elements determine not only the contribution of the emission from each volume element to the overall detected signal but also the changes in the shape of the fluorescence spectrum due to the dispersion of the absorption coefficient of the medium (Fig. 5). The spectral distortion of the fluorophore emission ensures that the above system of linear equations is nondegenerate and that the tomography problem can be solved.

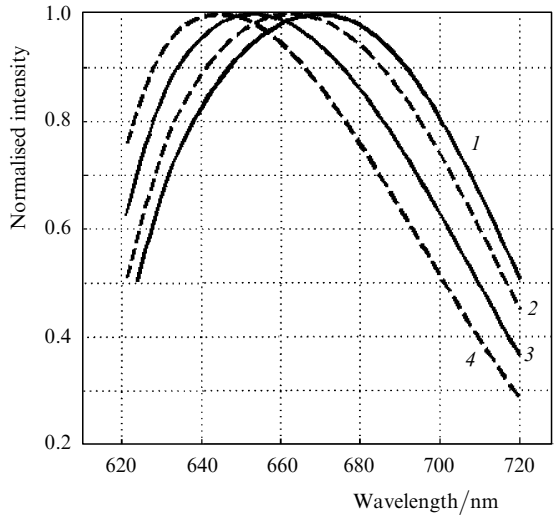

Figure 5. Normalised fluorescence spectra of TurboFP635 in a volume element at a depth $z = 0.5$ (*1*), 2.5 (*2*), 5.5 (*3*) and 8.5 mm (*4*) for a given point in the scan area ($x = 6$ mm, $y = 16$ mm).

The system of Eqns (6) is underdetermined because the spectral distortion due to the autofluorescence of the tissue is *a priori* unknown. Since the $A(\lambda)$ spectrum in general cannot be measured, the original system reduces to a parametric one:

$$P_{ij}^{s}(\lambda_m) - G(\lambda_m) P_{ij}^{d}(\lambda_m) = \sum_{k=1}^{n} K(x_i, y_j, z_k) F(\lambda_m)$$
$$\times [f_{ij}(z_k, \lambda_m) - G(\lambda_m) f_{ij}(d - z_k, \lambda_m)], \qquad (8)$$

where

$$G(\lambda_m) = \frac{\sum_{k=1}^{n} f_{ij}(z_k, \lambda_m) N(x_i, y_j, z_k)}{\sum_{k=1}^{n} f_{ij}(d - z_k, \lambda_m) N(x_i, y_j, z_k)}$$

is a parameter of the spatial distribution of autofluorescent inclusions for a wavelength λ_m.

The system of linear equations (8) has a set of solutions, each corresponding to a particular $G(\lambda)$ function. Clearly, physically possible solutions meet the constraint of a nonnegative fluorophore concentration. It should also be taken into account that the number of nonzero fluorophore concentrations should be minimal because the fluorophore can only be present in a small region (fluorescent proteins are present only in the tumour region), and the rest of the object does not emit. Thus, in the entire region of $G(\lambda)$ values corresponding to nonnegative fluorophore concentrations, the solution to the problem corresponds to the $G(\lambda)$ that minimises the number of nonzero $K(x_i, y_j, z_k)$ values. Using the method proposed in this study for fluorophore distribution reconstruction, we detected and localised a fluorescing tumour in a laboratory animal.

Figure 6 presents a 3D image of a fluorescing tumour in the form of virtual sections at different depths in the imaging subject. As seen, the cross-sectional dimensions of the fluorescent region correlate with the size of the tumour, which was imaged in reflected light and was located at depths from 1.5 to 4.5 mm (thickness of the object, 12 mm). The results were verified after removal of the tumour (post mortem). A 3D image of the tumour ($11 \times 25 \times 12$ mm, 1-mm spatial resolution) was obtained from the distortion of the measured fluorescence spectrum using a single projection of the imaging subject. This demonstrates the feasibility of using the proposed 3D reconstruction algorithm in SFDT.

5. Conclusions

Information about the shape of the emission spectrum allows one to more accurately determine the fluorophore distribution in the imaging subject in solving the inverse tomography problem, because the dispersion of the optical properties of biological tissue leads to characteristic changes in the shape of its fluorescence spectrum. The optimal spectral range for SFDT imaging of biological objects 1–2 cm in thickness is 600–700 nm, which offers a sufficiently high dispersion of the absorption coefficient in combination with a relatively weak integrated attenuation of light. The proposed SFDT method takes advantage of the dispersion of the absorption coefficient of biological tissues.

The prototype SFDT system described here is intended for imaging fluorescently labelled tumours in laboratory animals. Owing to the use of a common fibre output of the light sources and a single fibre input of the detector, in conjunction with an electromechanical scanner, the system has a relatively simple design and is inexpensive compared to its analogues. It was used to perform the first *in vivo* experiments aimed at localising a fluorescing tumour in a laboratory animal.

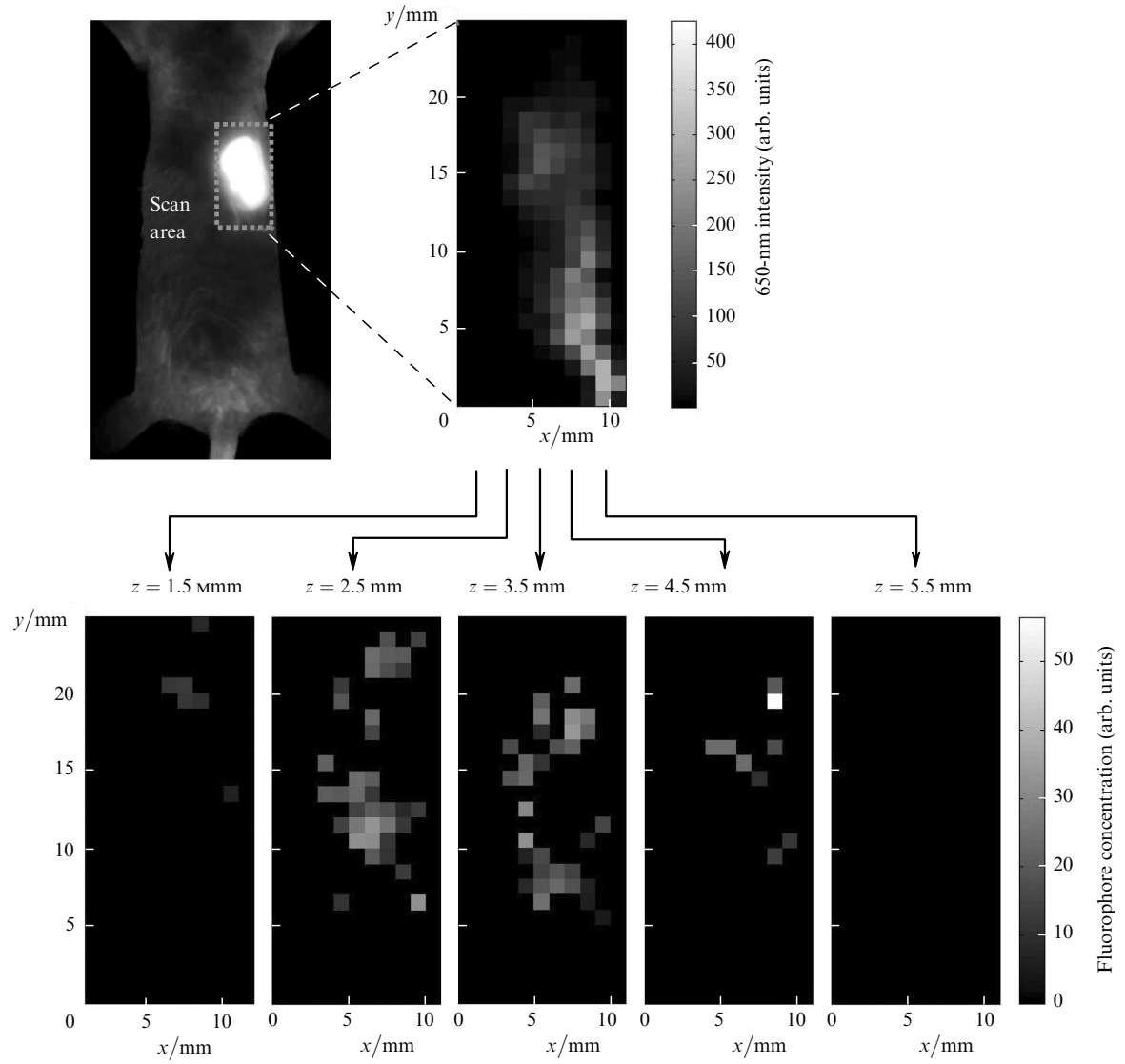

Figure 6. Reconstructed fluorophore distribution in an imaging subject (nude mouse with a TurboFP635-labelled tumour).

The proposed reconstruction algorithm enables 3D imaging of a fluorescing tumour from the distortion of the measured fluorescence spectrum using a single projection of the imaging subject. The first experimental results demonstrate that SFDT is a viable approach to tumour detection and localisation in laboratory animals with allowance for the autofluorescence of biological tissue. Clearly, the reconstruction quality can be significantly improved by using several SFDT projections.

Note that, in this study, light propagation in biological tissue was described in the widely used diffusion approximation of the radiative transfer equation for a homogeneous medium. The use of more adequate mathematical models will enable detection and localisation of fluorescent regions with higher accuracy.

Acknowledgements. We are grateful to S.M. Deev (Bach Institute of Biochemistry, Russian Academy of Sciences, Moscow) and I.V. Balalaeva (Lobachevski State University, Nizhnii Novgorod) for giving us the opportunity to perform experiments on laboratory animals with fluorescent-protein-labelled tumours. We are also indebted to V.A. Kamensky for his valuable suggestions and helpful discussions.

This work was supported by the Russian Foundation for Basic Research (Grant Nos 07-02-01262 and 10-02-01109), the Presidium of the Russian Academy of Sciences (Principles of Basic Research in Nanotechnologies and Nanomaterials Programme) and the Federal Agency for Science and Innovation (Project No. 02.740.11.0086).

References

1. Hoffman R.M. *Lab. Anim.*, **31**, 34 (2002).
2. Ntziachristos V., Turner G., Dunham J., Windsor S., Soubret A., Ripoll J., Shih H.A. *J. Biomed. Opt.*, **10**, 064007 (2005).
3. Turchin I.V., Kamensky V.A., Plehanov V.I., Orlova A.G., Kleshnin M.S., Fiks I.I., Shirmanova M.V., Meerovich I.G., Arslanbaeva L.R., Jerdeva V.V., Savitsky A.P. *J. Biomed. Opt.*, **13**, 041310 (2008).
4. Tret'yakov E.V., Shuvalov V.V., Shutov I.V. *Kvantovaya Elektron.*, **32**, 941 (2002) [*Quantum Electron.*, **32**, 941 (2002)].
5. Kravtsenyuk O.V., Lyubimov V.V., Kalintseva N.A. *Kvantovaya Elektron.*, **36**, 1043 (2006) [*Quantum Electron.*, **36**, 1043 (2006)].

6. Tuchin V.V. (Ed.) *Opticheskaya biomeditsinskaya diagnostika* (Optical Biomedical Diagnostics) (Moscow: Fizmatlit, 1998).
7. Kumar A.T., Raymond S.B., Dunn A.K., Bacskai B.J., Boas D.A. *IEEE Trans. Med. Imaging*, **27**, 1152 (2008).
8. Konovalov A.B., Vlasov V.V., Kalintsev A.G., Kravtsenyuk O.V., Lyubimov V.V. *Kvantovaya Elektron.*, **36**, 1048 (2006) [*Quantum Electron.*, **36**, 1048 (2006)].
9. Godavarty A., Eppstein M.J., Zhang Ch., Theru S., Thompson A.B., Gurfinkel M., Sevick-Muraca E.M. *Phys. Med. Biol.*, **48**, 1701 (2003).
10. Svensson J., Andersson-Engels S. *Opt. Express*, **13**, 4263 (2005).
11. Deliolanis N.C., Kasmieh R., Wurdinger T., Tannous B.A., Shah K., Ntziachristos V. *J. Biomed. Opt.*, **13**, 044008 (2008).
12. Axelsson J., Svensson J., Andersson-Engels S. *Opt. Express*, **15**, 13574 (2007).
13. Ripoll J., Yessayan D., Zacharakis G., Ntziachristos V. *J. Opt. Soc. Am.*, **22**, 546 (2005).
14. Contini D., Martelli F., Zaccanti G. *Appl. Opt.*, **36**, 4587 (1997).
15. Shcherbo D., Merzlyak E.M., Chepurnykh T.V., Fradkov A.F., Ermakova G.V., Solovieva E.A., Lukyanov K.A., Bogdanova E.A., Zaraisky A.G., Lukyanov S., Chudakov D.M. *Nat. Methods*, **4**, 741 (2007).